Scattered Wave Packet Formalism with Markovian Outgoing Wave Boundary Conditions for Open Quantum Systems

Chia-Chun Chou* and Robert E. Wyatt†

Institute for Theoretical Chemistry and Department of Chemistry and Biochemistry, The University of Texas at Austin, Austin, Texas 78712, USA

(Received 16 March 2011; published 11 July 2011)

The scattered wave formalism is developed for a quantum subsystem interacting with the external environment through open boundaries. The total wave function is divided into incident and scattered components and Markovian outgoing wave boundary conditions are applied to the scattered wave function. This formalism significantly reduces the computational effort relative to other methods which rely on Green functions and memory kernels. The method is applied to one-dimensional barrier scattering and to a three-dimensional model for the field effect transistor.

DOI: 10.1103/PhysRevLett.107.030401 PACS numbers: 03.65.Yz, 03.65.Nk, 73.63.−b, 85.30.Tv

Studies of open quantum systems require boundary conditions that allow for the exchange of matter and energy with the environment. Various open-system boundary conditions for the time-dependent Schrödinger equation (TDSE) have been designed to mimic a finite spatial domain coupled to external regions [1–6]. For example, a multistage wave packet propagation algorithm was recently applied to electrical conduction in a donor-bridge-acceptor system [7]. In addition, non-Markovian boundary conditions which employ Green functions and memory kernels have been used for model problems [4]. The complexity of some of these methods results in their being too time consuming for use in multidimensional applications.

In this study, a straightforward method requiring minimal computational effort is presented for introducing open boundary conditions into the solution of the TDSE for a quantum subsystem. In the scattered wave formalism, the total wave function is split into incident and scattered parts and outgoing wave boundary conditions are applied to the scattered wave function. The incident wave can be analytically propagated in the conduction channel or it can be injected through one of the surfaces where outgoing boundary conditions are applied to the scattered wave. The boundary conditions are not treated using effective Hamiltonians, negative imaginary absorbing potentials, Green functions, or memory kernels. The Markovian boundary conditions used here only require the form of the scattered wave function near the boundaries at the current time. It will be demonstrated in this study that the scattered wave method can be orders of magnitude faster than methods employing memory kernels.

The type of application well suited for the scattered wave formalism is the modeling of nanoscale electronic devices, including waveguides and channels [8,9], molecular wires [10,11], resonant tunneling diodes [12,13], and field effect transistors [14–17]. Quantum effects become significant in these devices and ballistic transport is frequently assumed because of the very short transit times in the conduction channel. In order to model the operation of these devices, the TDSE must be solved in the conduction channel with open boundary conditions at the interfaces to the external leads.

In a one-dimensional case, the time evolution of the wave function is described by the TDSE

$$i\hbar\frac{\partial\Psi(x,t)}{\partial t}=-\frac{\hbar^2}{2m}\frac{\partial^2\Psi(x,t)}{\partial x^2}+V(x)\Psi(x,t). \quad (1)$$

In the scattered wave formalism, we separate the total wave function into incident and scattered parts, $\Psi(x,t)=\Phi(x,t)+\Upsilon(x,t)$. The initial condition for the wave function is given by $\Psi(x,0)=\Phi(x,0)$. The incident wave function satisfies the free-space TDSE, and is launched from the left side of the conduction channel. Substituting the free-space TDSE into the TDSE for the total wave function in Eq. (1), we obtain the modified TDSE for the scattered wave function

$$i\hbar\frac{\partial\Upsilon(x,t)}{\partial t}=-\frac{\hbar^2}{2m}\frac{\partial^2\Upsilon(x,t)}{\partial x^2}+V(x)\Upsilon(x,t)+V(x)\Phi(x,t), \quad (2)$$

where the initial condition is given by $\Upsilon(x,0)=0$. The last term serves as an inhomogeneous source for the scattered wave function. The scattered wave function describes the outgoing waves created in the interaction region of the potential. In general, it is straightforward to analytically or numerically determine the incident wave function by solving the free-space TDSE. After obtaining the source term in Eq. (2), we solve the modified TDSE for the scattered wave function.

One important feature of the scattered wave formalism is that open boundary conditions can be applied to the scattered wave function to significantly reduce the size of the computational domain. The ratio method will be introduced for imposing open boundary conditions at the edges of the system. We assume that the computational domain $[\alpha,\beta]$

for the scattered wave function is discretized by $N + 1$ grid points x_k with $x_0 = \alpha$ and $x_N = \beta$. Outgoing wave boundary conditions are applied to the scattered wave function at the left and right boundaries. At the left boundary, the scattered wave function has the form of an outgoing wave, $\Upsilon(x) = \Upsilon_0 \exp(-ikx)$, provided that we have a constant potential outside the computational domain. Here, the coefficient Υ_0 and the wave vector k may be complex valued. From this condition, we can derive an equation associated with the scattered wave at the left three internal grid points, $\Upsilon(x_0) = \Upsilon(x_1)^2/\Upsilon(x_2)$. Thus, the scattered wave function at the left boundary can be determined from the scattered wave function at the interior points x_1 and x_2. We can derive a similar condition for the scattered wave at the right boundary. The outgoing wave boundary condition for the total wave function was previously applied to deep tunneling during proton emission [18]. A significant advantage of the scattered wave formalism is that different boundary conditions can be used for Φ and Υ at the same point. For example, at the left boundary, outgoing conditions can be imposed upon Υ while Φ is entering the internal region.

In order to demonstrate features of the scattered wave formalism, computational results will be presented for three model problems. The first of these concerns a Gaussian wave packet scattering from the Eckart barrier $V(x) = V_0 \mathrm{sech}^2(\gamma x)$, where $V_0 = 1.0$, $\gamma = 2.0$ (see Fig. 1). All quantities are given in atomic units in this example ($m = 1$ and $\hbar = 1$). The initial Gaussian wave packet is given by $\Phi(x) = g(x, 0) = (2\beta/\pi)^{1/4} \times \exp[-\beta(x - x_0)^2 + ip_0(x - x_0)/\hbar]$, where $\beta = 0.6$, $p_0 = 1.5$, and $x_0 = -5.0$. The incident wave function satisfying the initial condition and the free-space TDSE is known analytically [19]. The analytical expression for the time evolving Gaussian was used in the source term for the integration of the modified TDSE in Eq. (2).

The modified TDSE was solved for the scattered wave function from $t = 0$ to $t = 22$ using the leapfrog method with $\Delta t = 0.0025$ [20]. The computational domain was chosen so that $(x_0, x_N) = (-3, 3)$ with the spacing $\Delta x = 0.1$. Figure 1(a) displays the probability densities at $t = 4$ for the incident, scattered, and total wave functions. This figure shows that the reflected and transmitted wave packets are clearly separated and the reflectionless wave packet propagation through the boundaries has been achieved. If the wave function was reflected by the boundaries, interference effects in the probability density would be noted. In addition, the total wave function ($\Psi = \Phi + \Upsilon$) is in excellent agreement with the exact result obtained by solving the TDSE using a large spatial grid without employing open boundary conditions.

Figure 1(a) also shows the total wave function obtained by solving the non-Markovian TDSE [4] (the time step is $\Delta t = 10^{-5}$). Since this approach includes convolution integrals over the history of the system involving the Green functions for the reservoirs (the region outside the computational domain) and these Green functions display strongly oscillatory behavior, the need for a small time step to accurately estimate the memory integrals greatly increases the computational effort even for one-dimensional problems. Therefore, the scattered wave formalism can be several orders of magnitude faster than the integration of the non-Markovian TDSE.

Figure 1(b) shows the time-dependent probability flux at the left and right boundaries. Initially, the wave packet starts outside the computational grid, and then it enters the grid and interacts with the potential barrier. The gradual vanishing of the probability flux at the two boundaries indicates that as time progresses the resulting reflected and transmitted wave packets completely leave the computational grid without reflecting from the boundaries. Also, the probability flux obtained from the scattered wave formalism is in excellent agreement with the exact

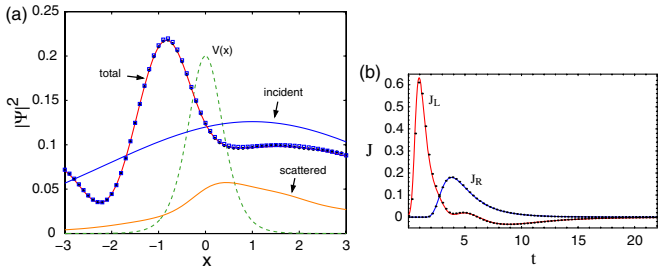

FIG. 1 (color online). (a) The incident, scattered, and total wave functions obtained from the scattered wave formalism (●). The wave functions obtained from the integration of the TDSE using a large spatial grid (curves) and from the non-Markovian TDSE (□) with the Eckart barrier in arbitrary units (dotted line) at $t = 4$. (b) The probability flux at the boundaries obtained from the scattered wave formalism (●) and from the integration of the TDSE using a large spatial grid (curves).

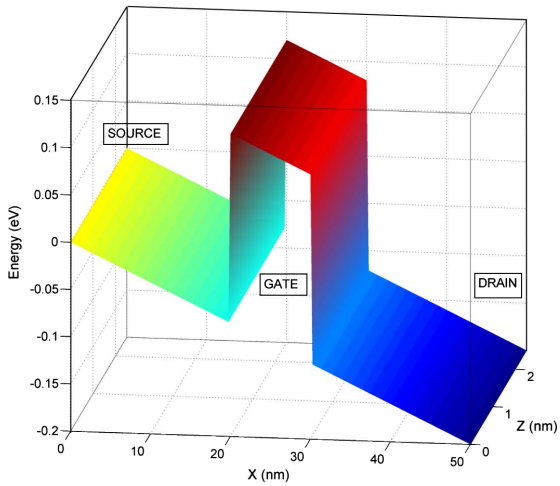

FIG. 2 (color online). Potential energy diagram in the channel region for the transistor model. The potential energy is shown for the vertical (x, y) slice at the middle of the channel along the y direction. The left side connects to the source electrode from which the incident wave packet is launched, the right side leads to the sink electrode, and the gate occupies the region along the x direction between 20 and 30 nm.

result. The absence of numerical reflections at the boundaries presents clear evidence for the validity of the outgoing wave boundary conditions.

In the second application of the scattered wave formalism, the transport of a quantum wave packet in the conduction channel of a field effect transistor will be computed. The channel region has dimensions along (x, y, z) given by 50 nm $\times$ 2.5 nm $\times$ 2.5 nm. In this region, a lattice of grid points was introduced, with 201 points along the channel axis and 11 points in each of the two transverse directions.

The initial wave packet launched from the source region is defined as the product of a Gaussian function along the x direction multiplied by ground state wave function for a two-dimensional box: $\Phi(x, y, x, t = 0) = g(x, t = 0) \times \chi(y, z)$. For the Gaussian function, the parameters are $E_x = 0.06\,\mathrm{eV}$ (translational energy), $\beta = 0.6 \times 10^{17}$ (width parameter), $x_0 = -8$ nm (center of wave packet), and the effective mass is m_0 (free electron mass).

In this study, the potential energy in the channel region is defined by the boundary conditions: the source region is grounded, the electric potential in the drain region is 0.2 V, and the gate is biased at -0.2 V. The resulting potential energy function shown in Fig. 2 displays a ramp leading from the source down to the drain with a superimposed rectangular barrier in the gate region. This electron potential energy is similar to that used in previous computational models [12,15–17].

The scattered wave packet in Eq. (2) was propagated by introducing an injection boundary condition for the incident wave function. In this approach, the time dependence of the incident packet was calculated on the boundary surface separating the source region from the conduction channel. Then, using the injected function as a source term for Eq. (2), both the incident function and the scattered function were propagated through the conduction channel. The outgoing wave boundary condition was applied to Φ only on the right (channel-drain) boundary, but this type of boundary condition was applied to Υ on both the left and right boundary surfaces. In particular, the following equation was used to compute the scattered wave function on the left boundary: $\Upsilon(0, y, z) = \Upsilon(\Delta x, y, z)^2/\Upsilon(2\Delta x, y, z)$. A similar condition was employed at the right boundary of the channel region.

Computational results were obtained for propagation times up to 650 fs. In Fig. 3, isosurface plots are shown for the real part of the scattered wave packet at 3 times: 3(a) 175 fs; 3(b) 225 fs; 3(c) 300 fs. These isosurfaces were drawn for values given by $\pm 0.05\gamma$, where γ is a convenient

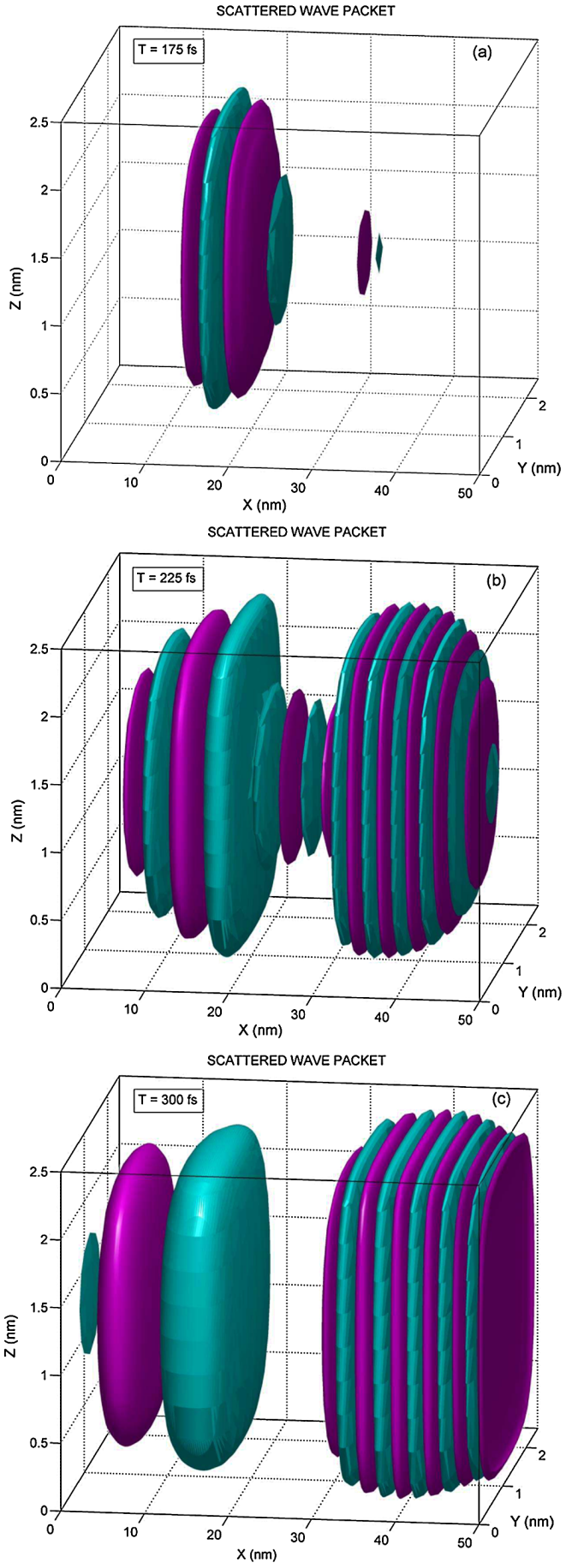

FIG. 3 (color online). Isosurface plots for the scattered wave packet at three times: (a) $T = 175$ fs, (b) $T = 225$ fs, (c) $T = 300$ fs. Surfaces are drawn for positive [dark gray (red)] and negative [light gray (cyan)] values of the real part of this wave function. These isosurfaces are plotted for the values $\pm 0.05\gamma$ where γ is a scale factor defined in the text.

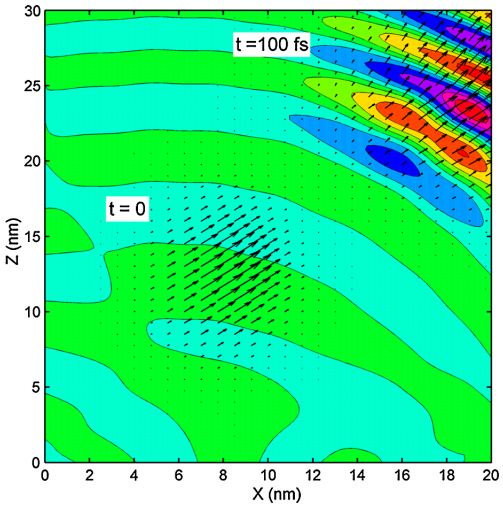

FIG. 4 (color online). Flux vectors for a wave packet propagating in a 2D region are shown at $t = 0$ and $t = 100$ fs. The initial packet is launched toward the step potential, which begins at $z = 25$ nm. At the later time, the contour map of real (Ψ) and the flux map show that the packet has partially transmitted the transparent boundaries along the top and right edges. The ratio method applied along the normal vectors to the two boundary surfaces accurately describes propagation through these surfaces.

scale factor, $\gamma = 4 \times 10^{13}$. The scattered wave packet is created at earlier times on the left side of the gate region, but in 3(a) the scattered wave is starting to form on the drain side of the gate. In 3(b), the scattered wave has built up on the drain side of the gate and a reflected component continues to form on the source side of the gate region. These two parts are connected by a smaller diameter tube extending through the gate region. In 3(c), this tube has disappeared from view and the components to the left and right of the gate are moving through the transparent boundaries into the source and drain regions.

In the previous examples, when crossing open boundary surfaces wave packet propagation occurred parallel to the surface normals. In the final example, flux vectors for the propagating packet make oblique contact with two boundary surfaces. Figure 4 shows flux vectors for the initial packet in a 2D region. The potential energy is zero except for the region $z \geq 25$ nm, where $V = -0.03$ eV. This wave packet is launched toward the upper right corner with a wave vector given by $k_x = 1.15$ nm^{-1} and $k_z = 1.02$ nm^{-1}. As time proceeds, the wave function is required to vanish along the left and lower boundaries, but the right and top boundaries are open. The figure also shows a contour map and flux vectors for the packet at $t = 100$ fs as it exits the transparent boundaries, where the ratio method was applied along the direction normal to each boundary surface. These results are in excellent agreement with those obtained by direct propagation in a much larger 2D region. The ratio method thus describes oblique propagation through boundary surfaces.

Some features of the scattered wave formalism are as follows. The scattered wave function is solved on a reduced computational grid involving only the interaction region of the potential with outgoing wave boundary conditions on surfaces leading to the source and drain regions. At each time step, the scattered wave function at the interior grid points is employed to determine this function at the boundaries. Unlike non-Markovian approaches involving memory kernels [4], prior values of the wave function at the boundaries are not required to determine the current wave function at the boundaries. In addition, this formalism can be readily applied to other open quantum systems in higher dimensionality without calculating the Green functions for different contacts. As demonstrated in the current study, the scattered wave formalism allows accurate, efficient, and stable computations for long-time propagation. Additional computational results will be described in future publications.

We thank the Robert Welch Foundation (Grant No. F-0362) for their financial support of this research.

*chiachun@mail.utexas.edu
†wyattre@mail.utexas.edu

[1] C. Leforestier and R. E. Wyatt, J. Chem. Phys. **78**, 2334 (1983).
[2] R. Kosloff and D. Kosloff, J. Comput. Phys. **63**, 363 (1986).
[3] A. Vibók and G. G. Balint-Kurti, J. Chem. Phys. **96**, 7615 (1992).
[4] J. R. Hellums and W. R. Frensley, Phys. Rev. B **49**, 2904 (1994).
[5] M. Mangin-Brinet, J. Carbonell, and C. Gignoux, Phys. Rev. A **57**, 3245 (1998).
[6] C. A. Moyer, Am. J. Phys. **72**, 351 (2004).
[7] A. B. Pacheco and S. S. Iyengar, J. Chem. Phys. **133**, 044105 (2010).
[8] Z. Chen, Y. Zhang, and Z. Yu, Chin. Phys. Lett. **26**, 037303 (2009).
[9] A. Jüngel and J. Mennemann, Math. Comput. Simul. **81**, 883 (2010).
[10] R. Li, J. Zhang, S. Hou, Z. Qian, Z. Shen, X. Zhao, and Z. Xue, Chem. Phys. **336**, 127 (2007).
[11] I. Franco, M. Shapiro, and P. Brumer, J. Chem. Phys. **128**, 244906 (2008).
[12] O. Pinaud, J. Appl. Phys. **92**, 1987 (2002).
[13] Y. Hou, W. P. Wang, N. Li, W. L. Xu, W. Lu, and Y. Fu, Appl. Phys. Lett. **93**, 132108 (2008).
[14] R. Venugopal, M. Paulsson, S. Goasguen, S. Datta, and M. S. Lundstrom, J. Appl. Phys. **93**, 5613 (2003).
[15] Y. Fu, M. Willander, and H. Pettersson, Appl. Phys. A **77**, 799 (2003).
[16] Y. Fu and M. Willander, J. Appl. Phys. **97**, 094311 (2005).
[17] E. Fernandez-Diaz, A. Alarcon, and X. Oriols, IEEE Trans. Nanotechnol. **4**, 563 (2005).
[18] M. Rizea, J. Math. Chem. **48**, 55 (2009).
[19] A. Goswami, *Quantum Mechanics* (Waveland Press, Long Grove, 2003).
[20] A. L. Garcia, *Numerical Methods for Physics* (Prentice Hall, Upper Saddle River, 1999).